CONF-920474--1

DE92 007234

Instrumentation and Controls Division

# AN ANALYSIS OF THE RELATIONSHIP BETWEEN INDUCTION MOTOR CURRENT AND SHAFT SPEED FLUCTUATIONS*

C. H. Nowlin
Oak Ridge National Laboratory
P. O. Box 2008
Oak Ridge, TN 37831-6006

Article to be submitted for presentation and publication at the
46th Meeting of The Mechanical Failures Prevention Group
Virginia Beach, VA
April 7-9, 1992



*Research Sponsored by the U. S. Department of Energy and performed at Oak Ridge National Laborataory, Managed by Martin Marietta Energy Systems, Inc. for the U. S. Department of Energy under Contract No. DE-AC05-84OR21400.

MFPG MANUSCRIPTS

FOR CAMERA-READY-COPY: Type single space full measure up to but not beyond the blue lines
Do not indent paragraphs, separate paragraphs with two lines.

# AN ANALYSIS OF THE RELATIONSHIP BETWEEN INDUCTION MOTOR CURRENT AND SHAFT SPEED FLUCTUATIONS*

C. H. Nowlin

Oak Ridge National Laboratory
P. O. Box 2008
Oak Ridge, TN 37831-6006

**Abstract:** For induction motors, motor shaft speed variations accompany motor load torque variations and motor torque variations. Hence, shaft speed fluctuation detection can serve as a warning of undesirable motor load conditions. This paper presents a theoretical foundation for the relationship between motor shaft speed fluctuations and stator current fluctuations when the shaft speed is perturbed by any cause. In addition, it shows that amplitude and frequency demodulation of motor current enhance the observed current fluctuations. The equations presented herein are derived in an as-yet unpublished work. Differential equations and basic electromagnetic equations, rather than phasors, are emphasized in their derivation. Fourier spectra of motor current, amplitude-demodulated motor current, and frequency-demodulated motor current are given for motor shaft speed modulated simultaneously with 13- and 17-Hz perturbations. We conclude that frequency demodulation is potentially a much better method to detect shaft speed fluctuations than is amplitude demodulation but that better methods of frequency demodulation are needed. The best presently available methods of frequency demodulation alias interference lines down into the spectra of interest below 60 Hz. There, they mask the valid spectral lines.

**Key Words:** Amplitude demodulation; fault detection; fault monitoring; fourier spectra; frequency demodulation; motor current; shaft speed fluctuations; theory.

**Introduction:** For induction motors, changes in motor shaft speed spectra accompany motor load torque variations and motor supply torque variations. Hence, changes in motor shaft speed spectra can serve as an indication of changes of motor and load characteristics and can be used to help stabilize system operation. If the motor is, for instance, driving a compressor in a uranium-enrichment plant, the observation of a particular motor shaft speed spectrum might indicate "rotating stall" operation. This information can be used to initiate plant operation changes that eliminate this potentially damaging axial compressor flow abnormality.

Various methods have been implemented to measure motor shaft speed spectra. Although the tachometer is an excellent tool, its use requires direct connection to the motor shaft and requires low-level signal wires to be run from the motor to the control room. The accelerometer is another tool for measuring motor shaft speed spectra. It measures speed spectra indirectly by measuring the spectra of reaction forces on the motor housing caused by shaft speed fluctuations. This method also requires the installation of signal cables from the motor to the observation point.

*Research Sponsored by the U. S. Department of Energy and performed at Oak Ridge National Laboratory, Managed by Martin Marietta Energy Systems, Inc. for the U. S. Department of Energy Under Contract No. DE-AC05-84OR21400.

FOR CAMERA-READY-COPY: Type single space full measure up to but not beyond the blue lines
Do not indent paragraphs, separate paragraphs with two lines.

Motor current observation is a convenient way to detect motor shaft speed spectral changes, particularly where the motors are dispersed over a large area and operated from a control room, because no additional wires need be run to the motor. Motor current spectra can be measured with the same wires that connect to the ammeters in the control room.

Thompson et al.[1] implemented motor current analysis with a spectrum analyzer and demonstrated the capability of detecting broken rotor bars in running motors. Kryter and Haynes[2] observed motor current with a spectrum analyzer to infer the characteristics of the motor load which was a motor-operated valve; they used spectral enhancement and applied the concepts of pattern recognition to correlate observed spectra with known valve characteristics.

Kliman and Stein[3] wrote an excellent review paper of the theories and techniques employed in detecting faults in induction motors by motor current analysis. Smith[4] used phase demodulation to detect changes in various motor loads. He and his coworkers have used both direct observation of the demodulated waveform and spectral enhancement. Smith also uses pattern recognition to correlate observed motor current spectra with known motor characteristics.

The present work presents the theoretically derived equations for instantaneous motor current as a function of shaft speed and shaft position. In an unpublished work, I derived these equations with basic electromagnetic equations and differential equations rather than with phasors. The motor model is a two-pole, three-phase, four-wire, wye-connected induction motor. The rotor is modeled with only two rotor bars. A two-rotor-bar, two-pole motor is used, rather than a multibar, multipole motor, because it is simpler to analyze and its analysis is more likely to be productive. Later, if needed, the analysis can be extended to multibar, multipole motors.

The theoretically derived equations enable the calculation of the Fourier spectra of motor current, the Fourier spectra of ideal amplitude-demodulated motor current and the Fourier spectra of ideal frequency-demodulated motor current. These spectra are presented herein for the motor shaft speed modulated simultaneously with 13 and 17 Hz perturbations. Finally, the Fourier spectrum of the frequency-demodulated motor current is presented for the same shaft speed modulations when the motor current is demodulated with the best available frequency-demodulation technology.

**Theoretical background:** The ratio of total stator current $I_1$ to the peak stator power-line-frequency current $I_0$ is

$$I_1/I_0 = P(t)\ Cos\ (\omega_e t) - Q(t)\ Sin\ (\omega_e t) \tag{1}$$

where

$$P(t) = 1.0 + [K]\left[\omega_e - \dot{\theta}(t)\right]\left[\ Sin\ [2\theta(t)]\ \right] \tag{2}$$

$$Q(t) = \{K\}\ \{\ \left[\omega_{SO} - \dot{\theta}(t)\right] + \left[\omega_e - \dot{\theta}(t)\right]\left[Cos\ [2\theta(t)]\ \right]\ \}, \tag{3}$$

$$K = \frac{34.32\ \mu_o L_b^2 R_b}{4\pi\ L_S L_g \Omega_R} \tag{4}$$

FOR CAMERA-READY-COPY: Type single space full measure up to but not beyond the blue lines
Do not indent paragraphs, separate paragraphs with two lines.

and where $\theta(t)$ is the rotor shaft position, in radians, as a function of time $t$; $\dot{\theta}(t)$ is the derivative of $\theta$ with respect to time and is the rotor shaft speed; $\omega_{SO}$ is the steady-state motor shaft speed in radians per second; $\mu_0$ is the permeability of free space and is $4\pi \times 10^{-7}$ H/m; $L_b$ is the length of the rotor bars in meters; $L_S$ *is* the length of the stator winding in meters; $R_b$ is one-half the distance between the two rotor bars in meters; $\Omega_R$ is the resistance, in ohms, of both rotor bars in series; $\omega_e / 2\pi = f_e$ is the power line frequency in hertz, and $L_g$ is the length, in meters, of the air gap between the rotor and stator. The constant $K$ is different for various motors and could change if a catastrophe occurs but can be considered constant during a revolution of the motor shaft. For $\Omega_R = 1\ \Omega$, $L_S = L_b = 2$ m, $R_b = 1\ m$, and $L_g = 0.001$ m, $K = 6.86 \times 10^{-3}$ s.

Equations (1) through (4), which I derive in an as-yet unpublished work, describe a current wave that is both amplitude and frequency modulated. Ideal demodulation of such equations is best accomplished by using functional, analytic methods.

To enable analytic demodulation of the motor line current, Eq. (1) is recast as

$$I_1 / I_0 = [A(t)] \left[ Cos\ [\omega_e t + \psi(t)] \right] \tag{5}$$

where

$$A(t) = \{ [\ P(t)\ ]^2 + [Q(t)\ ]^2 \}^{1/2} \tag{6}$$

and where the current phase function is

$$\psi(t) = ArcTan\ [Q(t)/P(t)]. \tag{7}$$

Then, ideal amplitude demodulation of the motor current can be performed with Eq. (6), and ideal frequency demodulation of the motor current can be performed by calculating $\dot{\psi}(t)$ which is, as given by differentiating Eq.(7),

$$\dot{\psi}(t) = \left[ \frac{P(t)\ \dot{Q}(t) - Q(t)\ \dot{P}(t)}{[P(t)]^2 + [Q(t)]^2} \right] \tag{8}$$

with $\dot{P}(t)$ given by

$$\dot{P}(t) = \{K\} \{ \left[\omega_e - \dot{\theta}(t)\right] \left[2\dot{\theta}(t)\right] [\ Cos\ [2\theta(t)]\ ] - \left[\ddot{\theta}(t)\right] [\ Sin\ [2\theta(t)]\ ] \} \tag{9}$$

and $\dot{Q}(t)$ given by

$$\dot{Q}(t) = \{K\} \{ \left[-\ \ddot{\theta}(t)\right] + \left[\omega_e - \dot{\theta}(t)\right] \left[-2\dot{\theta}(t)\ \right] [\ Sin\ [2\theta(t)]\ ] - \left[\ddot{\theta}(t)\right] [\ Cos\ [2\theta(t)]\ ] \}. \tag{10}$$

FOR CAMERA-READY-COPY: Type single space full measure up to but not beyond the blue lines
Do not indent paragraphs, separate paragraphs with two lines.

With Eqs. (5) through (10), as well as further explicit information about the functional form of $\dot{\theta}(t)$, analytic frequency and amplitude demodulation of the motor current waveform can be accomplished fully.

**Motor Shaft Speed Modulation:** For our Fourier spectra study, we assume the motor shaft speed $\theta(t)$ to be a superposition of a constant $\omega_{so}$ and two sinusoidal functions. That is,

$$\dot{\theta}(t) = \omega_{so} \left[ 1 - M_1 \, Sin\,(\gamma_1 t) - M_2 \, Sin\,(\gamma_2 t) \right] \tag{11}$$

which implies

$$\theta(t) = \omega_{so} \left[ t + M_1/\gamma_1 \, Cos\,(\gamma_1 t) + M_2/\gamma_2 \, Cos\,(\gamma_2 t) \right]. \tag{12}$$

We call $M_1$ and $M_2$ the modulation indices. The shaft modulation frequencies are $\gamma_1$ and $\gamma_2$ Our definition of the modulation index differs from that given in texts on frequency modulation. There, modulation index is defined as $M\omega_{so}/\gamma$. We believe that our definition will be more productive for motor current demodulation because the modulation is inherently seen as a perturbation of the average, or steady-state, motor shaft speed.

We use two modulation frequencies in our study to determine the importance of intermodulation. Our data will show that intermodulation is very disruptive for amplitude-demodulated spectra but of no importance for frequency-demodulated spectra.

**Fourier Spectra**

For all of the spectra given here, $M_1 = M_2 = 0.01$. Furthermore, $\omega_{so}/2\pi = f_{so} = 59$ Hz, $\gamma_1/2\pi = f_{m1} = 13$ Hz, and $\gamma_2/2\pi = f_{m2} = 17$ Hz. We have chosen $L_s = L_b = 2$m, $R_b = 1$ m, and $L_g$, the length of the gap between rotor and stator, equal to 0.001 m. Finally, the electrical power line frequency $\omega_e/2\pi = f_e$ which, for a two-pole motor, is also the frequency of the rotating magnetic field induced by the three stator windings, is 60 Hz.

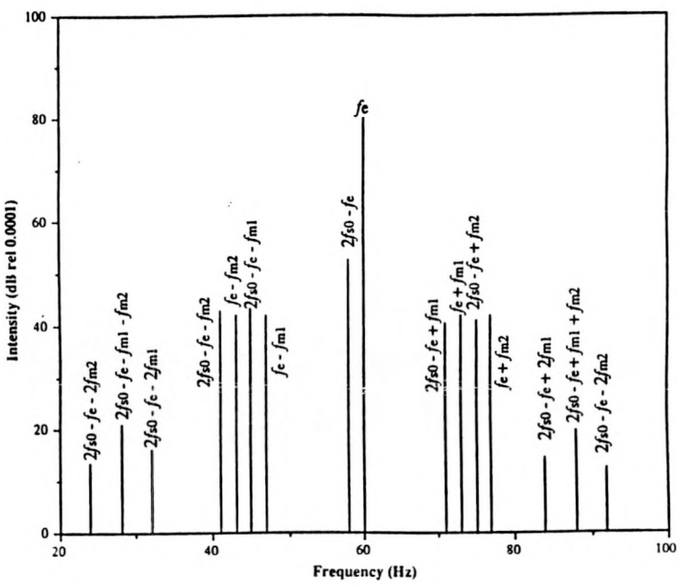


Fig. 1 Major Fourier Components of the Motor Currents.

FOR CAMERA-READY-COPY: Type single space full measure up to but not beyond the blue lines
Do not indent paragraphs, separate paragraphs with two lines.

**The nondemodulated Motor current spectrum:** For our set of system parameters, Fig. 1 shows the major Fourier spectrum of $I_1/I_o$ as given by Eq. (5). I define major components to be those more intense than 60 dB referenced to the most intense line of the spectrum. Although only the intensities of the spectral lines in dB are shown in Fig. 1, both the sine and the cosine coefficients, as well as the spectral line magnitude (the square root of the sum of the squares of the sine and cosine components) in dB, were computed. In Fig. 1, the spectral line component at the power line frequency is the strongest, as expected. However, the next most intense component is the one at 58 Hz, which is the same as two times the steady-state shaft rotation frequency minus the electrical frequency. If $\theta^{\bullet} = \omega_{so}$ in Eqs.(l) through (3), then standard trigonometric Identities show that this spectral line exists in the spectra even when the shaft speed is constant. Close examination of the other components shows that two groups of sidebands are interdigitated. One group consists of the sidebands of the 60 Hz carrier. The other group consists of the sidebands of the 58 Hz spectral line. Furthermore, we note that this lower 58 Hz sideband of the 60 Hz carrier does not have a matching upper sideband at 62 Hz. This single sideband at 58 Hz is consistent with that predicted by Eq. (1) of Kliman and Stein[3]. On the other hand, the sidebands for $f_{m1}$ and $f_{m2}$ do appear as pairs, and their cosine coefficients for the lower sidebands are the negative of those for the upper sideband. This condition is consistent with the presence of frequency modulation.

We note that for an actual operating motor, the nonlinear magnetic characteristics of the iron will likely cause sum and difference frequencies of the various components given in Fig. 1 to appear in the observed spectra. However, in this theoretical work, we assume the iron to be linear and we continue with the analytic demodulation of $I_1/I_o$ as given by Eq. (5).

**The ideal amplitude-demodulated spectrum:** Figure 2 shows the spectrum of the amplitude function $A(t)$, as defined by Eq.(6), for the same values of $\gamma_1$ and $\gamma_2$ and for the same modulation indices and other motor parameters as used for the spectrum shown In Fig. 1.

The most intense line in the spectrum is the one at $2f_{SO}$ . It has intense sidebands that carry amplitude and frequency modulation. These sidebands carry information about the modulation frequencies $f_{ml}$ and $f_{m2}$ as well as information about their harmonics and sum and difference frequencies. Most of these sidebands are outside the 0 to 60 Hz frequency band, which is the band of greatest interest to us .

One spectral line, the one at 2 ($f_{so}$ - $f_{m2}$), is potentially in the band below 60 Hz. Later in this paper, we will see that this same interference line appears in the ideal frequency-demodulated spectra. However, at this time, we move on to discuss the fatal flaw of even ideal amplitude demodulation.

The fatal flaw of even ideal amplitude demodulation of motor current is intermodulation distortion, which is evident in Fig. 2. The component at 4 Hz, which is the difference between the two modulation frequencies, and the component at 30 Hz, which is the sum of the two modulation frequencies are approximately as large as the components of the actual modulation frequencies of 13 and 17 Hz. Furthermore, the components at 26 and 34 Hz, which are the second harmonics of the modulation frequencies, are only 7 dB less than the components at 13 and 17 Hz. In summary, four spurious spectral lines and two real lines are in the portion of the spectrum below 60 Hz. Because of the presence of intermodulation distortion in the spectrum of Fig. 2, we end our discussion of ideal amplitude demodulation and move on to discuss ideal frequency demodulation.

FOR CAMERA-READY-COPY: Type single space full measure up to but not beyond the blue lines
Do not indent paragraphs, separate paragraphs with two lines.

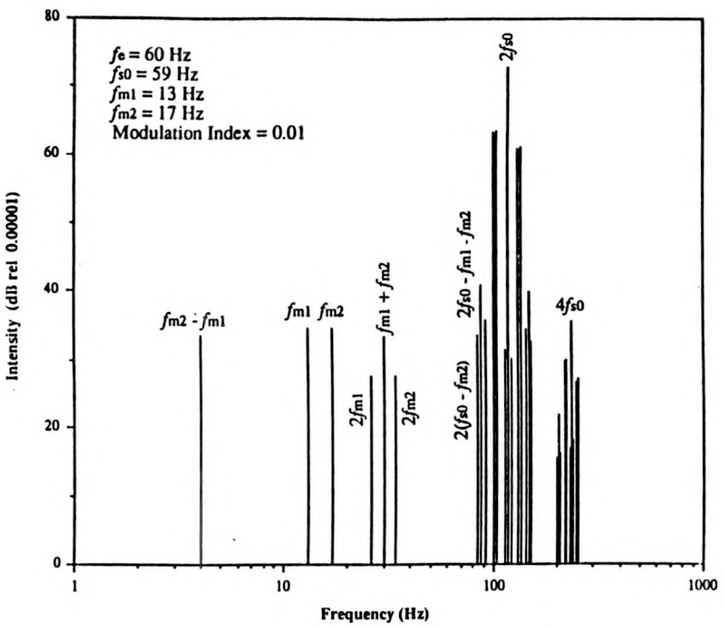


Fig. 2 Major Fourier Components of the Amplitude Demodulated Motor Current.

**The ideal frequency-demodulated spectrum:** Figure 3 shows the spectrum of the derivative of the phase function, $\psi(t)$, for the signal with the spectrum of Fig. 1.

In Fig. 3, the only significant components below 60 Hz are those for the shaft modulation frequencies of 13 and 17 Hz. There is no indication of any intermodulation of the 13 Hz and the 17 Hz modulation components. In Fig. 3, the intensities of the spectral lines at $f_{m1}$ and $f_{m2}$ are not equal even though the modulation indices are the same. The ratio of the intensity of the spectral line at $f_{m1}$ to the intensity of the line at $f_{m2}$ is exactly $f_{m1}/f_{m2}$ rather than 1. This discrepancy arises from our definition of modulation index combined with our decision to plot the derivative of the phase angle rather than the phase angle itself.

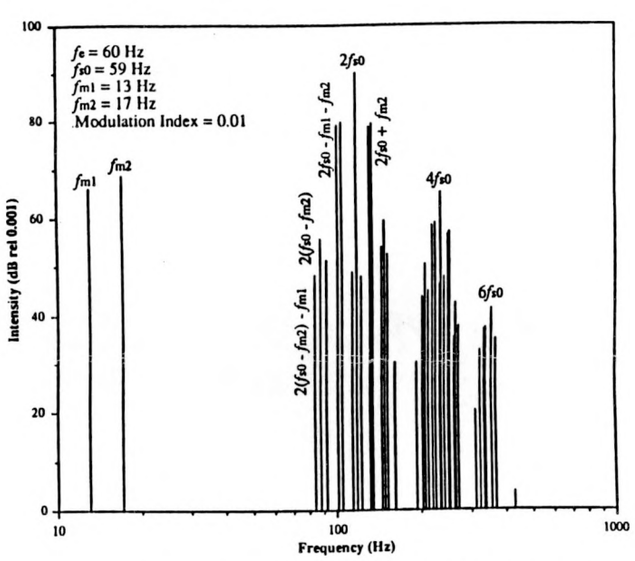


Fig. 3 Major Fourier Components of the Derivative of the Motor Current Phase Function.

Even though Fig. 3 shows no significant spectral lines below-60 Hz, attention must be given to the line at $2(f_{SO} - f_{m2})$ and what its presence may imply for other modulatlon frequencies. The intensity of this line is about 20 dB less than that for the companion line at $f_{m2}$. However, if its frequency were less than 60 Hz, it might be mistaken for a fundamental line of the motor shaft spectrum.

To determine the implications of this line, we define $f_{mm}$ to be the maximum modulating frequency of the motor shaft speed. Then, we define 0 to $f_c$ to be the frequency band of acceptable spectral lines for frequency-demodulated motor current. If

$$f_{mm} < f_{SO} - f_c/2 \ , \tag{13}$$

then the line $2(f_{SO} - f_{mm})$ lies above $f_c$. For $f_c = f_{mm}$, $f_{mm}$ must be less than $2f_{SO}/3$. For $f_{SO} = 59\ Hz$, $f_{mm} = f_c = 39\ Hz$. Hence, Eq. (13) indicates that, even for perfect frequency demodulation, the shaft speed spectra must be restricted to less than about 40 Hz to result in frequency demodulated motor current spectra that can be interpreted without ambiguity within a predefined frequency band. As previously mentioned, the intensity of this interference line appears to be about 20 dB less than that of its true companion. Furthermore, I observe from other spectra of ideal frequency-demodulated motor current that the intensity of this interference line seems to be reduced as $f_{mm}$ *is* increased.

We note in passing that an intense line is present in the spectrum of Fig. 3 at $2f_{SO} - f_{m1} - f_{m2}$. It may be that this line is a specific example of a generic line at

$$f_l = 2f_{SO} - \sum_{i=1}^{m} f_{mi} \tag{14}$$

where $f_{mi}$ is the i-th modulating frequency and $m$ is the total number of modulating frequencies. Further investigation is needed to determine whether the generic 1ine defined by Eq. (14) is always present with troublesome intensity for $m > 2$.

The most intense line in the spectrum of Fig. 3 is at 118 Hz. This frequency is $2f_{SO}$. The next most intense components are those at 101, 105, 131 and 135 Hz. These frequencies are precisely $2f_{SO} \mp f_{m1}$ and $2f_{SO} \mp f_{m2}$. Various other combinations of multiples of the $2f_{SO}$ subcarrier and the modulation frequencies are also present in the spectrum. Indeed, a rather intense line is present at $4f_{SO} = 236$ Hz and major components are at $6f_{SO} = 354$ Hz.

These spectral lines could be ignored except that all practical frequency-demodulation techniques are sampled-data systems and even the best available frequency-demodulation technology aliases these lines down into the frequency band below $f_e$ where they interfere with the true spectrum. To illustrate this universal characteristic of presently available frequency-demodulation technologies, we next examine the spectra of Fig. 1 after frequency demodulation with the best available technology.

**The frequency-demodulated spectrum obtained with the best-known technology:** All known methods of frequency demodulation applicable to a 60 Hz carrier are based on extracting the information contained in the zero crossings of the composite modulated signal. I disregard tuned-circuit demodulators such as the ratio detector and the discriminator because their behaviors are complex

and these methods of demodulation are not applicable to a 60 Hz carrier frequency modulated with higher frequencies. Furthermore, many commonly used methods of frequency demodulation introduce distortion as part of the demodulation process. For instance, the phase-locked loop method generates duration-modulated pulses as an intermediate step in the demodulation process. These duration-modulated pulses add harmonics of the original carrier and its sidebands to the final spectrum. To avoid the complications of these distortions while examining the effects of practical frequency demodulation, I demodulated the signal with the spectrum of Fig. 1 with a practical but distortionless demodulator. This practical demodulator does not cause additional distortion above that caused by the process of inspecting the nondemodulated signal at only its zero crossings.

This distortionless demodulator is a digital demodulator. It measures the time between successive zero crossings of the composite signal, takes the reciprocal of this difference, subtracts twice the carrier frequency, and outputs a signal proportional to the result. However, such a demodulator produces a sampled-data measure of the frequency of interest. It is well known that sampled-data measurement systems exhibit the property of frequency aliasing. Frequency aliasing refers to the appearance of spurious frequencies in the passband of sampled-data spectra whenever the true frequency is greater than half the sampling rate.

This distortionless demodulation process was applied to the function represented by the spectrum of Fig. 1. The spectrum that results from application of this sampled-data demodulation process is given in Fig. 4. In the frequency range below 60 Hz, the spectrum that results from the use of an ideal frequency demodulator, shown in Fig. 3, has only the actual modulation frequencies at 13 and 17 Hz. But the spectrum of Fig. 4 shows many other components that are aliased down from from their original positions above the sampling rate. Figure 4 shows lines at 2-Hz intervals through the frequency region. The component at 15 Hz, which results from the aliased components at 105 and 135 Hz in the Fig. 3 spectrum, is particularly intense. It is the second most intense component in the spectrum. The component at 19 Hz, which results from the aliasing of the line at 101-Hz in the analytic spectrum, is also intense. Even though at most only one combination of modulation frequency and carrier frequency are identified in Fig. 4, every spectral line, except for the lines at $f_{m1}$ and $f_{m2}$, is the result of a Fourier sum of many combinations of carrier and modulation frequencies. For instance, the line at 15 Hz results from components at $f_{m1} + 2(f_e - f_{so})$ and at $f_{m2} - 2(f_e - f_{so})$. The presence of the many spurious spectral lines, some as great as those reflecting actual shaft modulation, could seriously reduce the usefulness of frequency-demodulated motor current spectra.

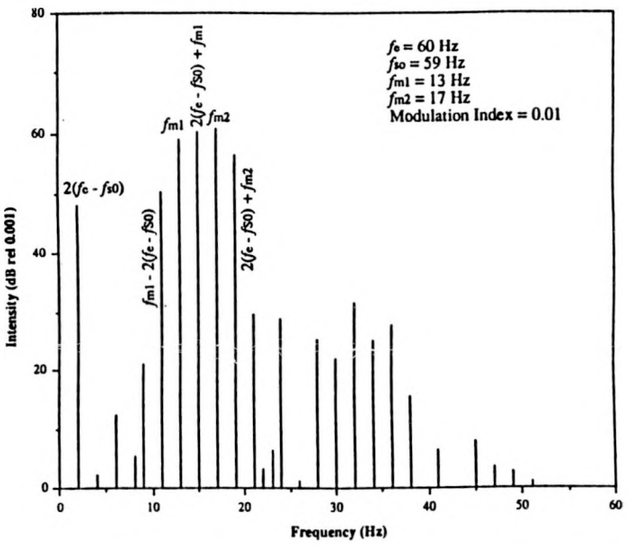


Fig. 4 Major Fourier Components of the Frequency-Demodulated Motor Current Demodulated With the Best Available Technology.

MFPG MANUSCRIPTS

FOR CAMERA-READY-COPY: Type single space full measure up to but not beyond the blue lines
Do not indent paragraphs, separate paragraphs with two lines.

Taken together, Figs. 3 and 4 show that better frequency demodulation methods are needed to reveal the full information that is contained in the frequency modulated data. Because the interference lines that are aliased down into the frequency region of interest, it would appear that these lines could be removed by the appropriate band-pass filters. However, study of the original non-demodulated spectrum of Fig. 1 shows that the interference lines are intermingled so closely with the valid lines that they cannot be separated by any band-pass filter applied to the original signal.

**Summary:** The spectra presented in this paper show that even ideal amplitude-demodulated motor current spectra contain a confusing mixture of real and extraneous lines. Although not within the scope of this paper, I have calculated spectra for square-law demodulators and for full-wave rectifier demodulators. For each of these demodulators, the spectra are more cluttered than those of the ideal amplitude demodulator. Further effort should not be spent developing amplitude-demodulated motor current systems for observing motor shaft speed fluctuations. However, there may be other applications where it is the preferred method of motor current demodulation.

On the other hand, our ideal frequency-demodulated motor current spectra have exactly the same lines as the motor shaft speed spectra for the frequency region below the electrical power frequency. However, threatening extraneous spectral lines are present in the ideal frequency-demodulated motor current spectra above the power frequency. Most importantly, with the best presently available frequency-demodulation methods, which are inherently sampled-data systems that sample at twice the power frequency, the spectral lines above the power frequency are aliased down into the frequency region below the power frequency. There, they mask the true spectral lines. To eliminate this problem, better frequency demodulation methods must be developed.

**Acknowledgments:** The author gratefully acknowledges the support of the Process and Long-Range Technical Support Program under the U. S. Department of Energy uranium enrichment activity throughout this work.

*References:*

1. W. T. Thomson, S. J. Chalmers, and D. Rankin, "An On-Line, Computer-Based Current Monitoring System for Rotor Fault Diagnosis in 3-Phase Induction Motors," *Turbomachinery International*, **17**, Nov/Dec, 1987, pp. 17-24.

2. R. C. Kryter and H. D. Haynes, "Condition Monitoring of Machinery Using Motor Current Signature Analysis," *Sound and Vibration*, **23** (No. 9), 1989, pp. 14-21.

3. G. B. Kliman and J. Stein, "Induction Motor Fault Detection via Passive Current Monitoring - A Brief Survey," *Proceedings of the 44th Meeting of the Mechanical Failures Prevention Group*, Virginia Beach, Virginia, April 3-5, 1990, pp. 49-65.

4. S. F. Smith, K. N. Castleberry and C. H. Nowlin, "Machine Monitoring Via Motor-current Demodulation Techniques," *Proceedings of the 44th Meeting of the Mechanical Failures Prevention Group*, Virginia Beach, Virginia, April 3-5, 1990, pp. 87-96.